



EXPERIMENTAL AND NUMERICAL INVESTIGATION OF THE BEHAVIOUR OF PILES IN SOFT SOILS UNDER MONOTONIC AND ALTERNATING LOADING

Michael Max BUEHLER¹, Roberto CUDMANI², Gerd GUDEHUS³

SUMMARY

The interaction of single vertical piles with soft soils during monotonic and cyclic loading is investigated with the FE-method. The piles have circular cross-sections and are assumed to be elastic. The mechanical behaviour of the neighboured soil is modelled with hypoplastic relations. For rate dependent materials the pile-soil-interface is modelled using a penalty formulation which allows large relative displacements, including a complete separation, i.e. the formation of gaps between the soil and the pile. The constitutive relation is introduced with the help of numerical simulations of drained and undrained element tests. A model test was carried out to investigate the flow resistance of piles in a creeping slope, and back-analysed. A numerical simulation of a creeping slope before and after stabilization with dowels is presented. A numerical model is proposed to calculate the creep induced horizontal loading of a pile foundation embedded in a soft soil slope at Kandla Port after the 2001 Gujarat/India earthquake. Finally a model pile in soft clay under alternating loading is presented in experiment and calculation. We can conclude that the proposed models are suitable for the interaction of piles and soft soils in static and dynamic problems.

CONSTITUTIVE RELATIONS

Two hypoplastic constitutive relations are employed in the present calculations: One for modelling of rate-independent behaviour of granular soils (e.g. sand), the other for rate-dependent materials with soft particles (e.g. clays). Both relations enable the description of the behaviour of soils under monotonic and cyclic loading. They incorporate the critical state concept of soil mechanics and the dependence of the stiffness on the current stress, density and history of deformation.

¹ Dipl.-Ing., Institute of Soil and Rock Mechanics, University of Karlsruhe, Germany.
Email: MichaelMax.Buehler@ibf.uni-karlsruhe.de

² Dr.-Ing., Institute of Soil and Rock Mechanics, University of Karlsruhe, Germany.
Email: Roberto.Cudmani@ibf.uni-karlsruhe.de

³ o.Prof. Dr.-Ing. Dr. h.c., Institute of Soil and Rock Mechanics, University of Karlsruhe, Germany.
Email: Gerd.Gudehus@ibf.uni-karlsruhe.de

Hypoplasticity

The hypoplastic constitutive law, firstly proposed by KOLYMBAS [8], is a tensorial rate-independent incrementally non-linear constitutive equation. The mathematical formulation requires neither a yield surface nor a flow rule, nor a decomposition of the strain rate into elastic and plastic parts. The rate of effective stress $\dot{\boldsymbol{\sigma}}'$ is a tensor-valued function of the rate of strain $\dot{\boldsymbol{\varepsilon}}$, and of three state variables: the current effective stress $\boldsymbol{\sigma}'$, the void ratio e and the so-called intergranular strain tensor $\boldsymbol{\delta}$ which takes into account the influence of the recent deformation history. The hypoplastic constitutive law can be represented most generally in the following form (1).

$$\dot{\boldsymbol{\sigma}}' = \mathbf{H}(\boldsymbol{\sigma}', e, \boldsymbol{\delta}, \dot{\boldsymbol{\varepsilon}}) \quad (1)$$

A representation of the function \mathbf{H} can be found in [12].

The solution of boundary value problems requires the determination of both material parameters and initial values of the state variables. The hypoplastic constitutive equation contains 13 material parameters. Material properties and the state variables void ratio e and stresses are strictly separated in our formulation. The material parameters are independent of the state variables. This enables the behaviour of a soil to be modelled in a wide range of stresses and densities with the same set of parameters. The hypoplastic parameters can be evaluated from *disturbed* soil samples using standard laboratory tests. For practical purposes they can also be estimated from results of index tests if size distribution, shape and hardness of grains are known [1], [6], [13]. This is a decisive advantage of hypoplasticity as against those elastoplastic models which use state dependent material parameters such as an elastic modulus, angle of friction and dilatancy. The initial void ratio can be determined directly from *undisturbed* soil samples (time consuming and expensive) or estimated indirectly from *in-situ* tests. For this purpose, a procedure for the interpretation of cone penetration and pressuremeter tests based on a hypoplastic cavity expansion model can be applied [4]. The initial stress state is determined from the weight of the overlying soil strata and assumed earth pressure coefficients.

Visco-hypoplasticity

NIEMUNIS [13] modified the hypoplastic model using NORTON's rule [14] to formulate a constitutive relation capable to model creep, relaxation, and rate dependent shear resistance of soft soil. The basic constitutive equation of the visco-hypoplastic model [13], [5] can be written in its most general formulation:

$$\dot{\boldsymbol{\sigma}}' = \mathbf{H}(\boldsymbol{\sigma}', e, \boldsymbol{\delta}, \dot{\boldsymbol{\varepsilon}}, \dot{\boldsymbol{\varepsilon}}_v) \quad (2)$$

All visco-hypoplastic parameters, i.e. compression index λ , swelling index κ ; exponent β , viscosity index I_v , critical friction angle φ_c , reference void ratio e_{100} , and reference strain rate D_r , can be determined from laboratory tests. The compression index λ and the swelling index κ are evaluated using the formulation proposed by BUTTERFIELD [3], which is describing the stiffness for isotropic first loading or normal consolidation (3), and subsequent unloading and reloading (4), respectively:

$$\ln\left(\frac{1+e_0}{1+e}\right) = \lambda \ln\left(\frac{p}{p_0}\right) \quad (3) \quad \ln\left(\frac{1+e_0}{1+e}\right) = \kappa \ln\left(\frac{p}{p_0}\right). \quad (4)$$

The exponent β is needed to define the ratio between the preconsolidation pressure and the cohesion. β also influences the stress response, i.e. shape of the stress path, for undrained shearing in saturated, normally consolidated soil. β is determined by means of undrained shear tests. The critical friction angle φ_c is determined using triaxial tests reaching critical state conditions, i.e. for sufficiently large strains. The viscosity

index I_v can be evaluated by using the semi-log compression index C_c and the index C_α for secondary consolidation [2],

$$I_v = \frac{C_c}{C_\alpha}. \quad (5)$$

The reference void ratio e_{100} is the void ratio of the NC-soil under isotropic stress of 100 kPa. The reference deformation rate D_r can be chosen as the strain rate for reference conditions, e.g. strain rates used in laboratory tests.

Calibration of the visco-hypoplastic relation for *Goldhausen* clay

The FE-investigation to be presented in the next section is based on laboratory tests and model tests with a clayey soil from *Goldhausen*/South-Western Germany [9], [18], [19]. The minerals are mainly kaolin, feldspar and quartz. Material properties of the *Goldhausen* clay can be taken from Table 1.

liquid limit w_L	plastic limit w_P	specific weight ρ_s	clay fraction $d < 2 \mu\text{m}$	Organic content
47%	18%	2.67 g/cm ³	65% by weight	6.3%

Tab. 1: Material properties of *Goldhausen* clay

Compression index λ , swelling index κ , reference void ratio e_{100} , and reference strain rate D_r

In order to determine the parameters λ and κ , load-controlled oedometric compression tests with *Goldhausen* clay are evaluated according to the Butterfield compression law. Figure 1 shows the results of four oedometric tests performed by KUNTSCHE [9]. Calculations were performed with different λ -values and the same κ -value. The values of λ and κ that fit the experiments best are $\lambda=0.125$ and $\kappa=0.01$.

An evaluation of the oedometric tests leads to $C_c=0.235$ and $C_s=0.02$. The reference void ratio is $e_r=0.949$ for an effective axial pressure of $\sigma_r=100$ kPa. To determine the compression index λ and the swelling index κ the double-logarithmic relations (3) and (4) are used.

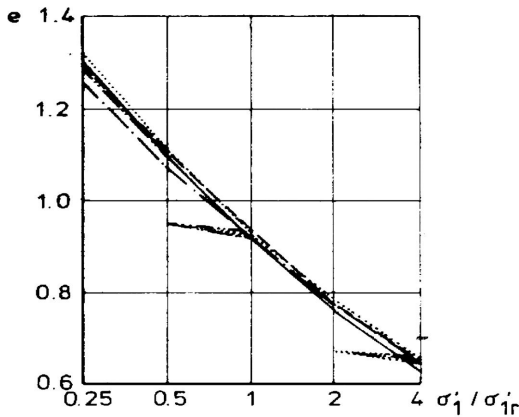


Fig. 1: Oedometric tests in semi-log [9]

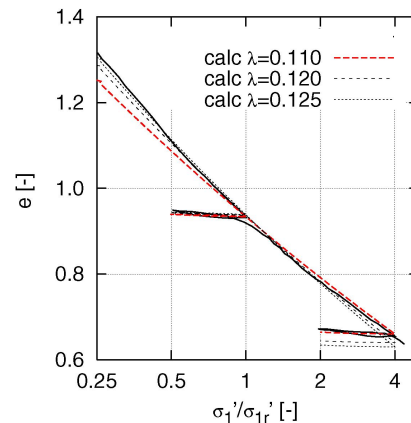


Fig. 2: Compression curves for $\lambda=0.110$, 0.120 , and 0.125 , respectively.

D_r can be directly determined by performing an oedometric test with constant strain rate. For load controlled tests the assumption is made that at the end of primary consolidation the creep rate is independent on the applied load. For our clay the strain rate at the end of primary consolidation time is $D_r=1.0E-05$.

Thus, the slope of the first compression curve is $\lambda=0.125$ while the slope of the unloading-reloading curve is $\kappa=0.01$. The reference void ratio is $e_{100}=0.941$ for an effective axial pressure of $\sigma'_v=100$ kPa.

Figure 2 shows the influence of a slight change of λ on the simulated soil response. A higher λ leads to a better agreement of experiments and calculations for low pressures whereas a smaller λ improves the agreement for higher pressures.

Viscosity index I_v

CIU triaxial tests with strain rate jumps can be used to determine the viscosity index I_v . Figure 4 shows that an increase of the strain rate during undrained shearing causes an increase of the deviatoric stress. LEINENKUGEL [10] proposed an empirical correlation relating the strain rate and the undrained resistance. The logarithmic viscosity law by LEINENKUGEL is given in (6) where $c_{u\alpha}$ and $\dot{\epsilon}_\alpha$ are reference values for the ultimate shear strength at a specific deformation rate:

$$\frac{c_u}{c_{u\alpha}} = 1 + I_v \ln\left(\frac{\dot{\epsilon}}{\dot{\epsilon}_\alpha}\right) \cong \left(\frac{\dot{\epsilon}}{\dot{\epsilon}_\alpha}\right)^{1/I_v} \quad (6)$$

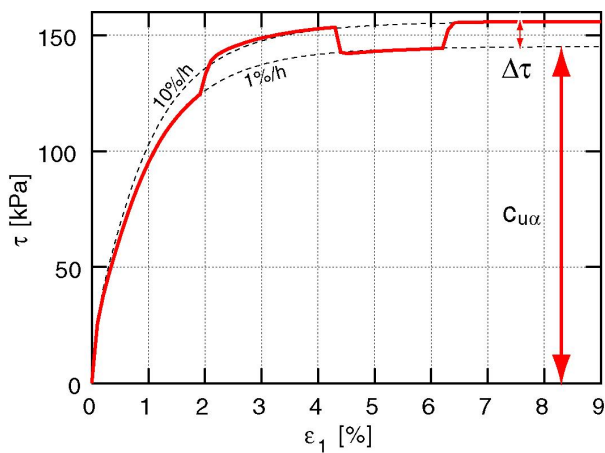


Fig. 3: Calculated change of shear strength after a change of deformation rate during CIU test

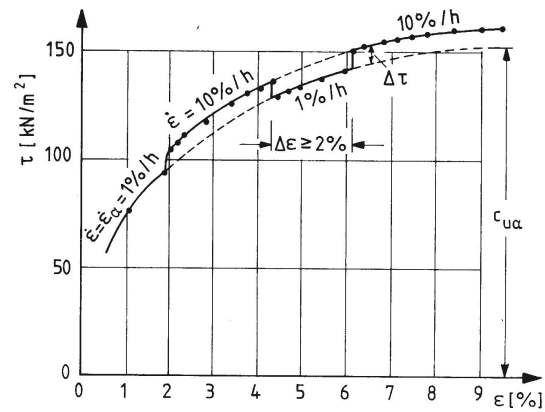


Fig. 4: Measured change of shear strength after a change of deformation rate during CIU test [10]

Applying equation (6) to the triaxial test results of Figure 4 we obtain a viscosity index $I_v = 3.1\%$ for *Goldhausen* clay. I_v can be estimated by means of an empirical correlation proposed by LEINENKUGEL [10] for different soft soils (Fig. 5).

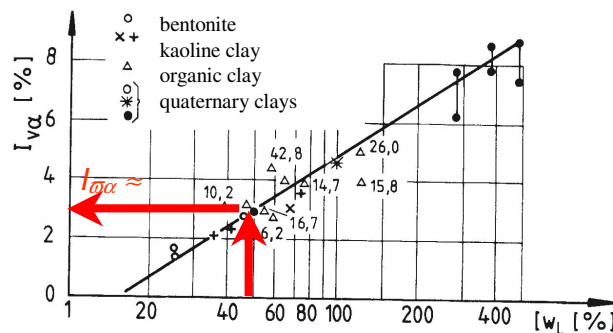


Fig. 5: Correlation between the viscosity index I_v and the liquid limit w_L [10]

Critical friction angle φ_c

In order to determine the critical friction angle results of CIU tests are used [9]. A constant strain rate $\dot{\varepsilon}=2.89\text{E-}05/\text{s}$ is applied in axial direction for both numerical calculations and experiments. Figures 6 and 7 compare experimental and calculated results. Measured pore pressures and reached deviatoric stress at the peak suit very well compared with the calculated CIU tests. Table 2 summarizes the determined material parameters for *Goldhausen clay*.

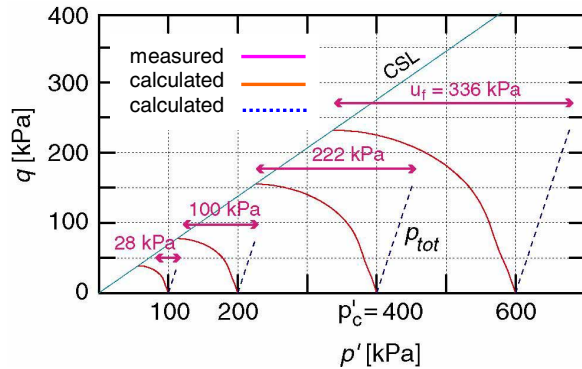


Fig. 6: Effective and total stress paths for different confining pressures. Measured pore pressures suiting perfectly.

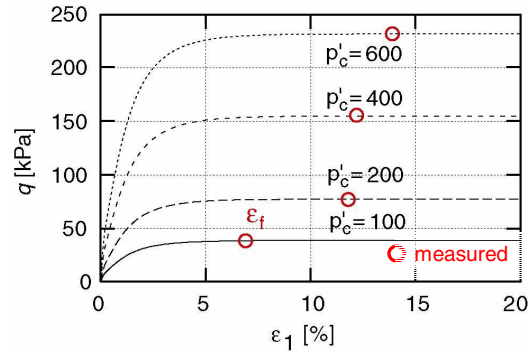


Fig. 7: Deviatoric stress q vs. axial strain ε_1 for different confining pressures. Peak at limit state ε_f from experiments.

e_{100}	λ	κ	β	I_v	φ_c	D_r	m_R	m_T	R	β_r	χ
0.914	0.125	0.01	0.85	0.031	18°	1.E-5	5.0	5.0	1.E-4	0.1	0.9

Tab. 2: Visco-hypoplastic parameters used in calculations

Numerical cyclic element tests with fixed deviatoric stress limits

Figure 10 shows numerical simulations of cyclic CU tests where the deviatoric stress is kept constant. The diagram at the left bottom reproduces the typical change of the hysteretic behaviour after one, 16, and 256 cycles, respectively. The deviatoric strain increases with growing number of cycles. The shape of the hysteretic curves are similar to the measurements (Fig. 9). The gradual decrease of the mean pressure over the number of cycles is also depicted (Fig. 10, right bottom) and can be well compared with the measured values (Fig. 9, top). The calculated curve resembles the expected butterfly curves, which can also be observed by plotting OCR versus deviatoric strain. Figure 10, diagram top left, shows that the range of the overconsolidation ratio is increasing with number of cycles.

Figure 12 shows numerical simulations of cyclic CU tests for the deviatoric strain kept constant. Also in case of the following boundary conditions the constitutive relation is working well by simulating realistic curves with decreasing mean pressure and deviatoric stress over the number of cycles (measurements in Figure 11).

FLOW RESISTANCE OF PILES

Introduction

To determine the flow pressure and flow motion of soil or the flow resistance of structures embedded in the soil a physical relation between shear stress τ and deformation rate $\dot{\varepsilon}$ is required. WINTER [19] developed a mathematical theory for the case of steady state and plain strain conditions. Based on research on the viscous behaviour of soft soils done by LEINENKUGEL [10], and first experimental and theoretical contributions on the flow resistance for piles by WENZ [17], WINTER [19] proposed an analytical solution for simple flow problems, particularly the creep of an extended slope.

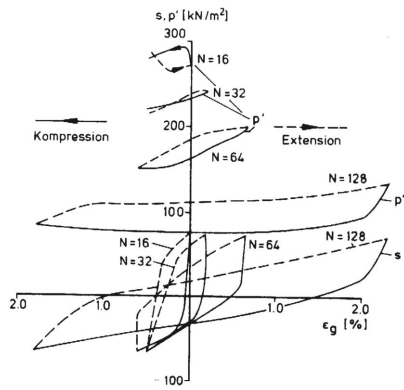


Fig. 8: Measured mean pressure (top) and deviatoric stress (bottom) vs. deviatoric strain [9].

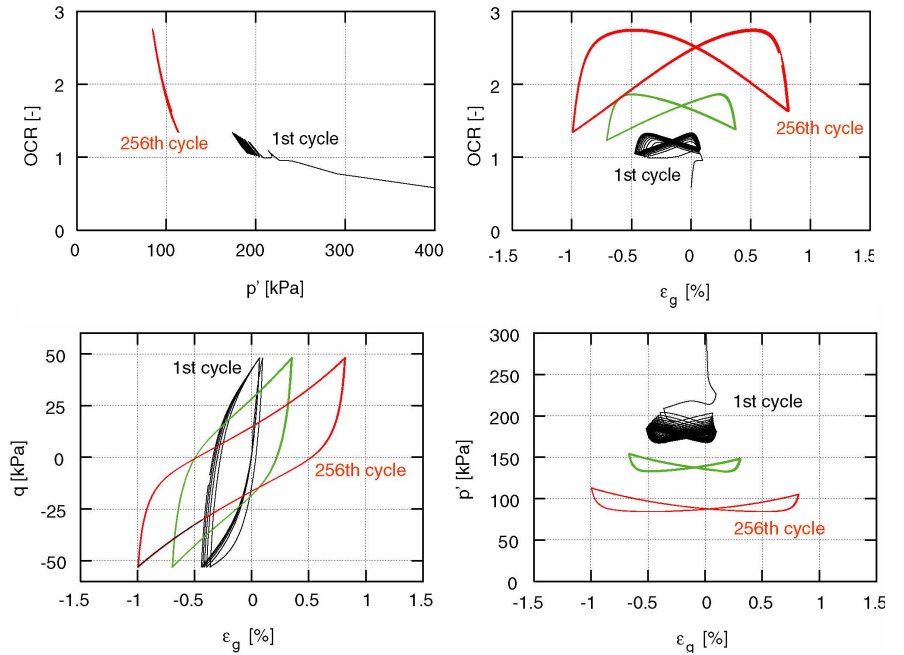


Fig. 9: Deviatoric stress q vs. deviatoric strain ϵ_g (bottom left), mean pressure p' vs. ϵ_g (bottom right), OCR vs. p' (top left), and OCR vs. ϵ_g (top right) after one and 256 cycles for constant with fixed deviatoric stress limits.

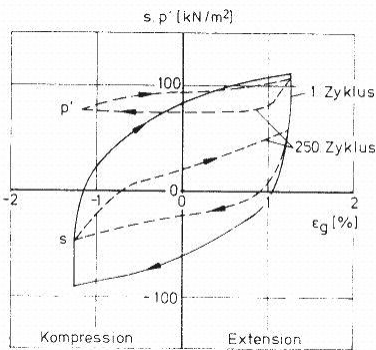


Fig. 10: Measured mean pressure (top) and deviatoric stress (bottom) vs. deviatoric strain [9].

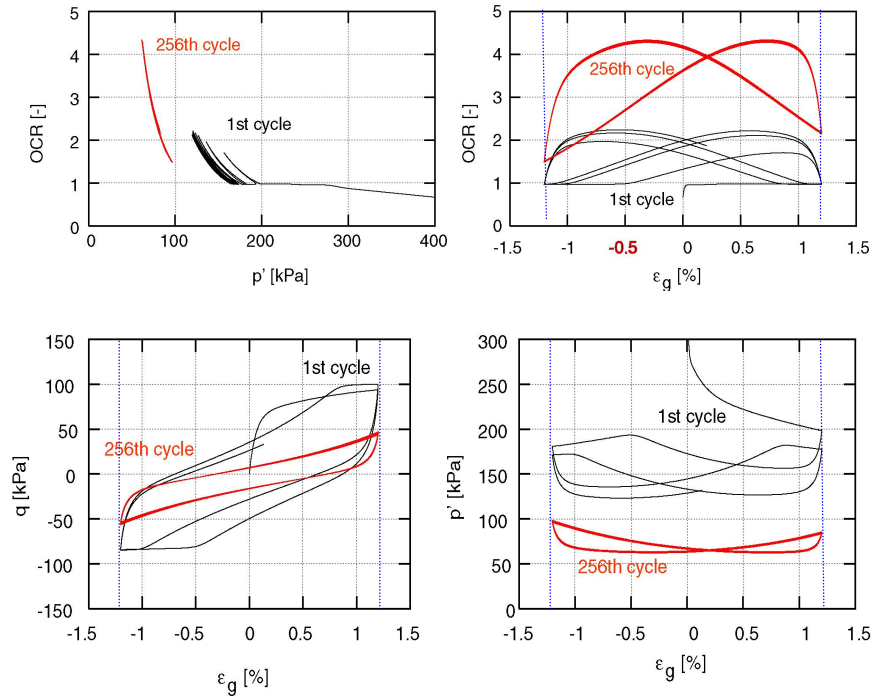


Fig. 11: Deviatoric stress q vs. deviatoric strain ϵ_g (bottom left), mean pressure p' vs. ϵ_g (bottom right), OCR vs. p' (top left), and OCR vs. ϵ_g (top right) after one and 256 cycles with fixed deviatoric strain limits

Theoretical dimensionless solution for the steady state flow resistance of piles

As a tool to dimension pile foundations and dowelled slopes WINTER developed a dimensionless solution for stationary plane and isochoric conditions with respect of the viscosity, i.e. creep, of clayey soils under homogeneous Dirichlet boundary conditions [18]. The dimensionless solution, developed by means of numerical and analytical methods, is formulated in equation (7). The flow rate \dot{u} is normalized by the reference strain rate D_r , whereas the flow resistance of the pile is normalized by $c_u d$ in which c_u is the undrained shear strength at a deformation rate $\dot{\epsilon} = D_r$.

$$\frac{p_f}{c_u d} = \kappa_F \left(\frac{\dot{u} / D_r}{a - d} \right)^{I_v} \quad (7)$$

For cylindrical piles the shape factor κ_F for different ranges of d/a is approximated by (8), (9). The shape factor κ_F also depends on the pile shape, the presented solution refers to a circular pile cross section.

$$\kappa_F = 4.83 \left(2.76 \frac{d}{a} + 1 \right) \quad \text{for } 0.1 < \frac{d}{a} < 0.5 \quad (8)$$

$$\kappa_F \approx 5.0 \quad \text{for } \frac{d}{a} < 0.1 \quad (9)$$

The structure of the presented solution resembles the constitutive law of the soil, i.e. the large scale answer (here to predict the flow resistance of piles) is directly related to the small scale answer obtained e.g. by numerical element tests. Later experiments and analytical considerations verified this concept.

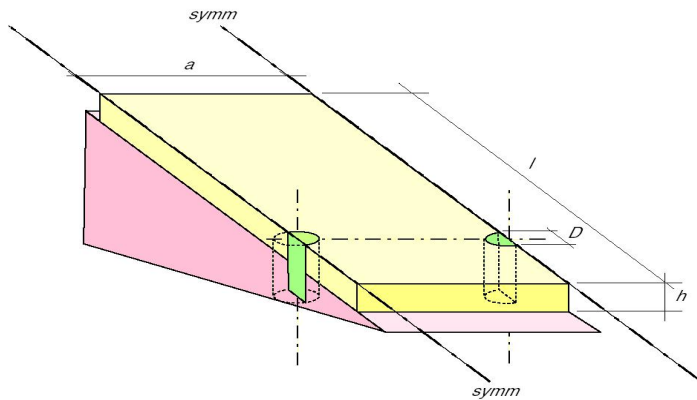


Fig. 12: Example of a 3D flow motion problem. Geometry of a finite piled slope

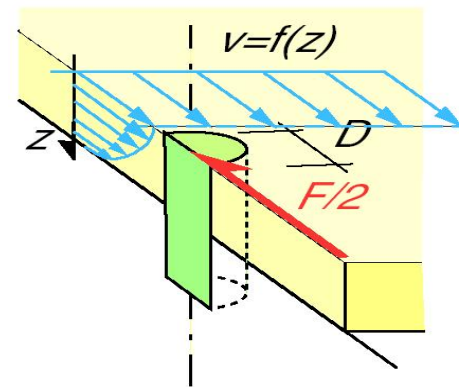


Fig.13: Typical flow profile of a creeping slope.

Small scale experiments to determine the flow resistance of piles

Introduction

Small scale model tests were carried out to delimit the practical area of validity of the dimensionless solution for steady state flow problems as well as to investigate the strain, so called flow deformation, to mobilize the maximum flow resistance. The flow deformation cannot be calculated with WINTER's approach, thus experiments or numerical calculations are required. Numerical calculations are able to take into account the pile shape, the installation geometry, the velocity and the properties of the viscous medium, the surface roughness of the pile, the *OCR* as well as the confining pressure, which has been strongly simplified in WINTER's solution.

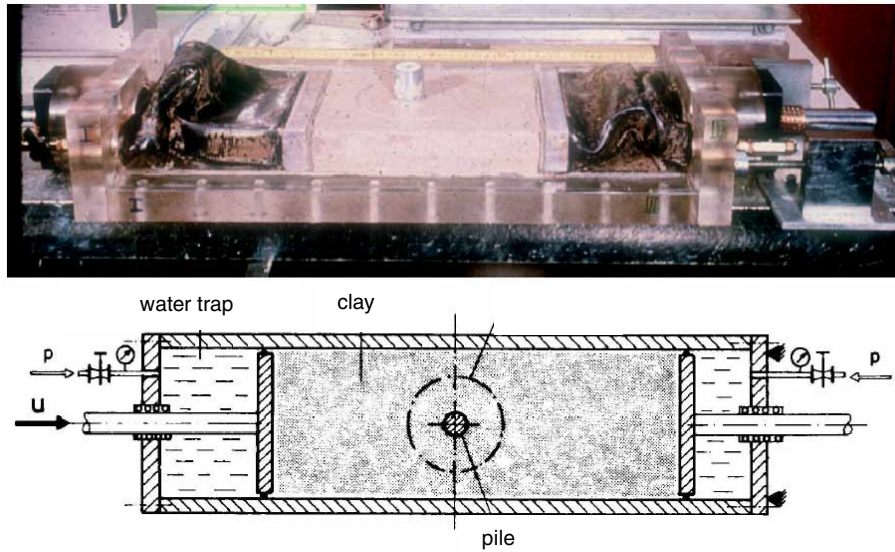


Fig. 14: Small scale model test to determine the flow resistance of piles [19]

Experimental setup

Soil samples used in the model tests were prepared by mixing clay powder with $w=1.6\%$ with distilled water under vacuum ($p=-90$ kPa) to obtain a viscous homogeneous suspension of $w\approx 100\%$ which is around two times the liquid limit.

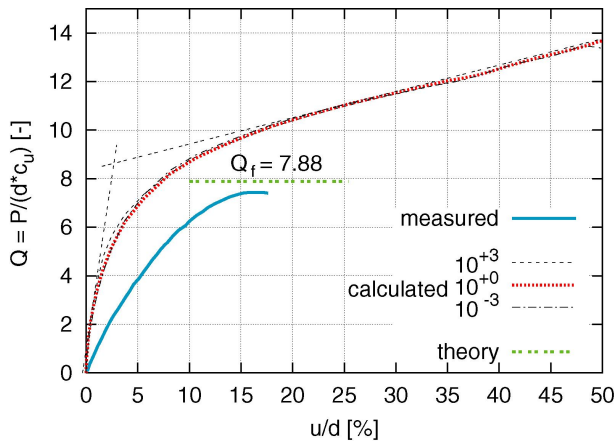


Fig. 15: Dimensionless solution of the numerical simulation compared with the measured and theoretical results

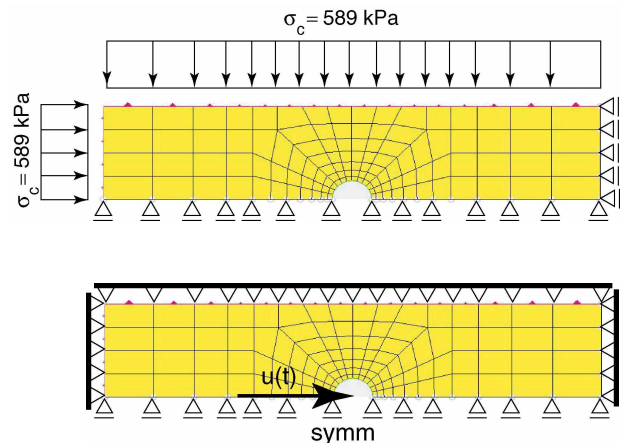


Fig. 16: FE-mesh for the numerical simulation. Initial conditions (top) and boundary conditions during the simulation.

At first the clay specimen is consolidated by means of an appropriate apparatus allowing drainage from the bottom and the top. The minimum consolidation time was around one week. The consolidation stress is applied incrementally by hydraulic jacks up to $p_c = 1000$ kPa. After completing of the consolidation process the specimen is cut to the dimensions of $50 \times 20 \times 20 \text{ cm}^3$. Subsequently it is mounted on the testing apparatus (Fig. 14) simulating plain deformation by moving the soil specimen relatively to the pile which is installed symmetrically. The lateral boundaries of the apparatus are lubricated. Chambers filled with water provide a horizontal pressure on two lateral boundaries of the specimen. Piles with different diameters can be installed, and the specimen can be shifted with different velocities along the pile while keeping a constant distance between the two lateral boundaries.

Numerical simulation of the experiment

The symmetry of the problem is taken into account by modelling half the system. Between pile and soil friction is set equal to zero, but gapping in the flow shadow of the pile is allowed as total stick is leading to unrealistic results and to numerical problems due to tensile stress in the continuum elements. The initial isotropic stress field is applied by loading two faces with the confining pressure of $\sigma_c = 589 \text{ kPa}$. Prior to the simulation step the boundaries are fixed in both directions except for the symmetry nodes, which are constrained perpendicular on the direction of motion.

The results are given in Figure 15. The numerical solution is depicted in a dimensionless term by dividing the diameter of the pile d and the undrained shear strength c_u evaluated by means of the presented numerical element test.

Dowelling of creeping slopes

Assuming a constant thickness of the shear zone during the creeping process the velocity of a creeping slope v is proportional to the rate of deformation $\dot{\epsilon}$. After installation of dowels in the slope the velocity of creep is decreasing from v_0 to v_1 . The shear stress in the shear zone is decreasing by an amount of

$$\Delta\tau = \tau_0 I_{v\alpha} \ln\left(\frac{v_0}{v_1}\right) \quad (10)$$

This concept is used for the stabilization of creeping slopes. The FE-simulation refers to a stabilization carried out at Stahlberg/Germany [15], [16], where 28 large dowels ($\varnothing 3.0 \text{ m}$) are used to stabilize a freeway embankment ($h=12\text{m}$) laying on a clayey slope (5° to 8°). The slope (260m width, 150m length) was observed by inclinometer measurements and geodetic measurements at its surface. After a filling of 10 m the slope set into motion. Firstly a ballast fill has been installed without any slow-down. Subsequently soil dowels have been installed like wells. Thereupon the slope stabilized from initial creeping rates at the surface of about 5 mm/month down to 1-2 mm/month.

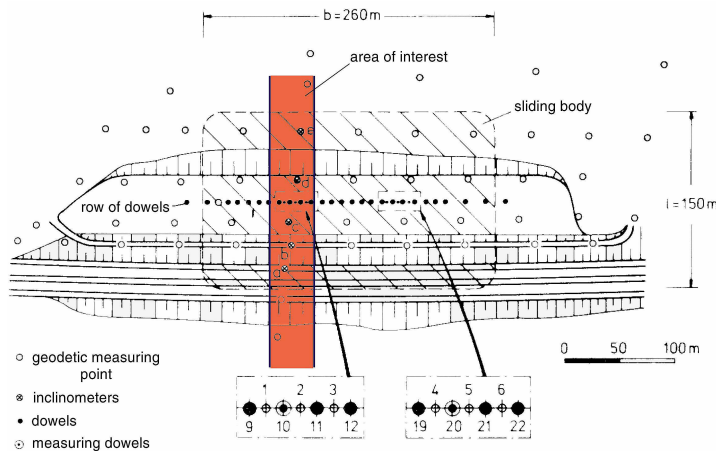


Fig. 17: Plan view on a stabilization of a creeping slope in the course of a freeway construction [15]

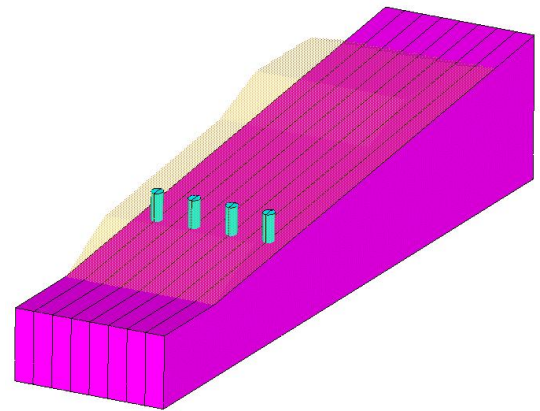


Fig. 18: Area of interest with installed dowels used for FE-calculations

The area of interest is simplified using symmetry planes through and between the dowels resulting in a FE-model consisting of half a pile. The calculations detect two primary sliding surfaces, one directly on the surface of the former slope and the other between a layer of soft ($c_{uo}=100 \text{ kPa}$) and underlying stiff clay ($c_{uo}=300 \text{ kPa}$). Conventional failure mechanisms [15] are verified by our FE-calculations by visualizing the in-plane shear deformations and magnitude of displacements.

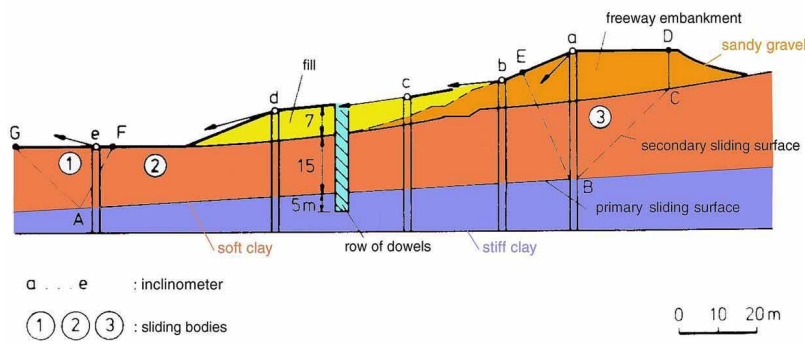


Fig. 19: Cross section of a stabilization of a creeping slope in the course of a freeway construction [15]

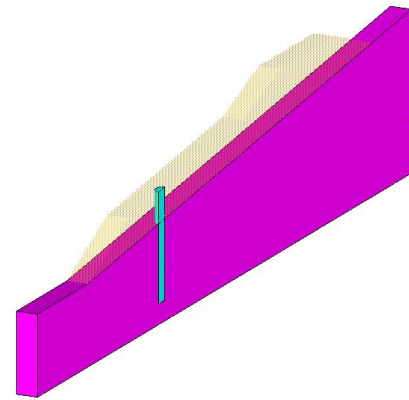


Fig. 20: FE-model with used symmetry planes

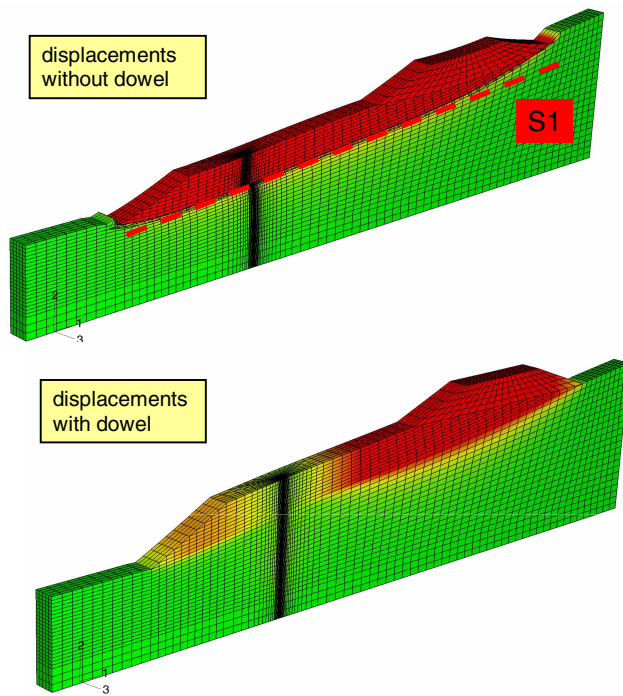


Fig. 21: Calculated displacements due to the filling of the freeway embankment with and without dowels (sliding surface S1)

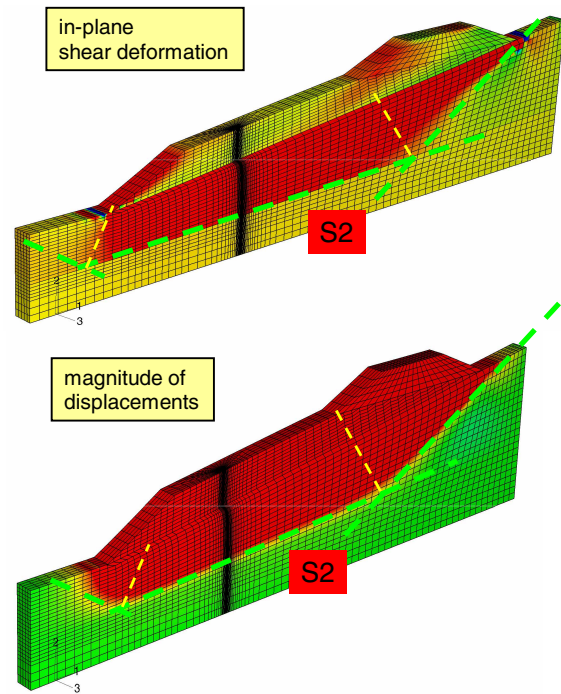


Fig. 22: Identified mechanisms due to filling of freeway embankment with deep sliding surface (S2) without dowels

Damages due to Soil-Foundation-Failure at Kandla Port/Gujarat/India

At 26th January 2001 a M6.9 earthquake of 90s destroyed shore constructions for berthing and loading platforms at the port of Kandla 40km south of the epicentre. The deep foundations consist of precast concrete spun piles driven through soft silty marine clayey sediments down to a sandy layer. After the earthquake cracks parallel to the shoreline were detected. Within a few months after the earthquake the cracks still grew in width will the soil in the hinterland sagged. Predominantly horizontal cracks were detected in 50% of the piles 10-30cm below the tie beam. It is supposed that the piles along the coast line were damaged by a combination of reasons. Firstly the piles were subjected to a lateral flow pressure on the piles punching beyond its weight due to a steepening of the coastal slope by sedimentation (1:1.5 instead of 1:3).

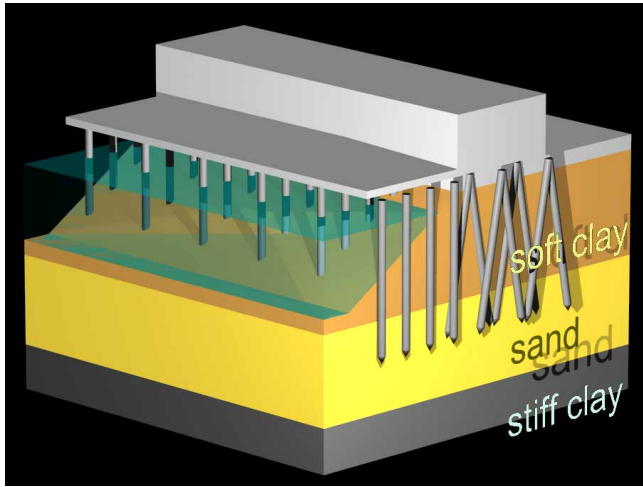


Fig. 23: Pile foundations for shore constructions for berthing and loading platforms at Kandla Port/India damaged during M6.9 earthquake

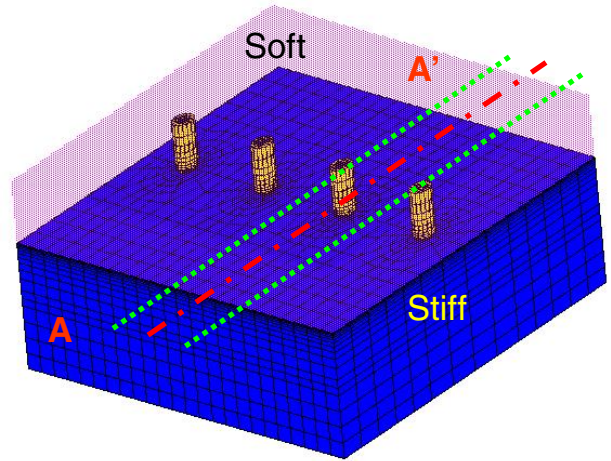


Fig. 24: FE-Model of row of piles, using symmetry planes and periodic boundary conditions for all nodes on plane A and A'

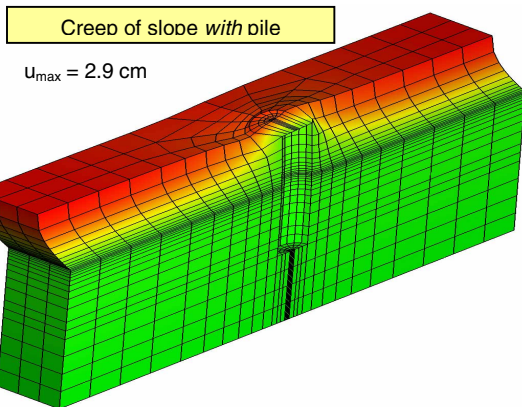
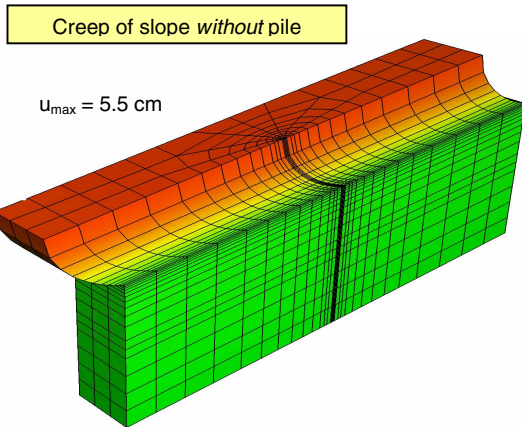


Fig. 25: Creep of slope with and without piles, magnitude of displacement after one year

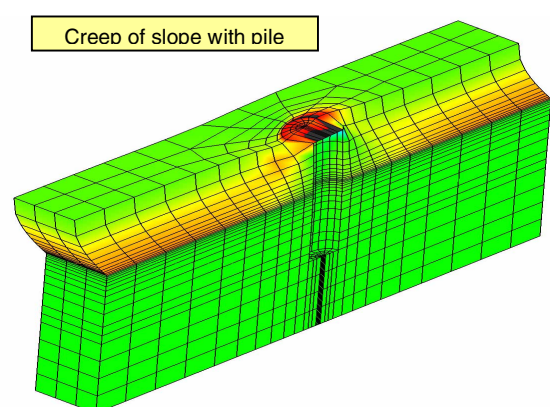
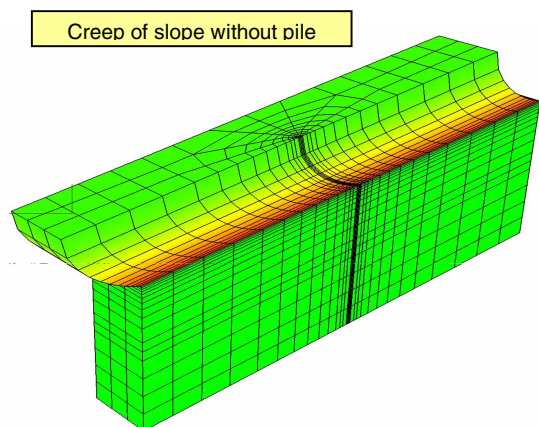


Fig. 26: Comparison of shear deformation in the slope with and without pile after one year

Secondly the strong ground motion was transmitted from the raker piles on the vertical piles by attracting horizontal forces. The slope lost its stability due to a temporary softening of the clayey soil induced by a pore pressure buildup during the earthquake.

The FE-simulation is carried out using a periodic boundary condition by letting all opposing nodes on the planes A and A', respectively, translating in the same manner. Also symmetry planes are taken into account according to the former model. A visco-hypoplastic material is used for soft and stiff clay. The state of the soil (excess pore pressure) can be used with free field conditions shortly after the earthquake event. A consolidation analysis could be carried out until the excess pore pressure is completely dissipated, subsequent calculated displacements are due to creep of the slope.

An evaluation of the FE-calculations show considerably higher creeping rate for creep without a pile foundation (with pile: 2.9cm/year, without pile: 5.5cm/year). This is expected due to the decrease of shear stress because of the pile in the shear zone. The reduction of shear stress in the shear zone is down to zero in the vicinity of the pile.

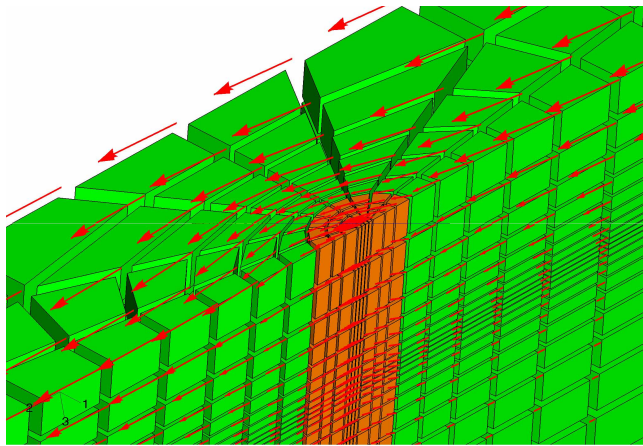


Fig. 27: Visualized vector field of displacements of the flow of soil along the pile

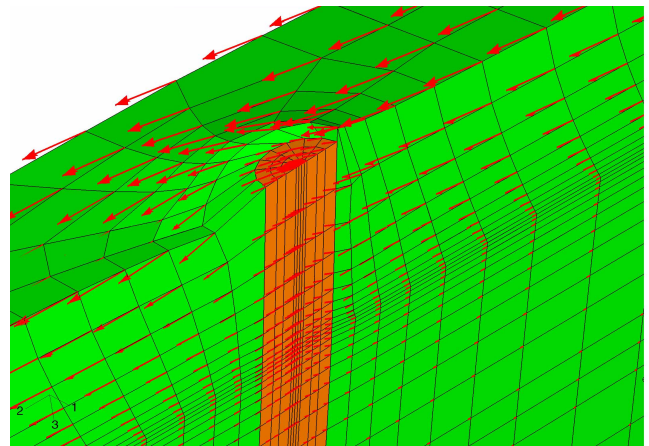


Fig. 28: Heave of soil above the pile and sunk of soil below the pile, gapping between soil and pile not allowed

Model pile subjected to lateral alternating loading

Figure 29 show a model test with a vertical lead pile carried out in a box. At first the elastoplastic and ductile pile was clamped in the middle of the box. Thereafter the box was filled with almost fully-saturated soft lacustrine clay until a horizontal surface 3 cm below the pile head was obtained. The pile head was subsequently loaded horizontally by means of a steal rope with a constant force in 1-direction. Perpendicular (in 2-direction) the pile head was subjected to a quasi-static alternating loading (Fig. 29a). As a result the pile head shifted gradually in direction of the constant load, i.e. in 1-direction. The experiment was back calculated by modelling the soil with visco-hypoplasticity and the pile with elasto-plasticity. The element mesh is shown in Figure 29b. Observed force displacement curves are depicted in Figure 29c, whereas Figure 29d shows the results obtained by the calculation.

CONCLUSIONS

The behaviour of piles in soft soils under lateral loading was investigated with the FE-Method using a visco-hypoplastic constitutive law. It was shown that monotonic element tests, e.g. oedometric compression, undrained triaxial shearing with strain rate jumps and different confining pressures can be simulated realistically. Also numerical element tests under cyclic loading show a satisfying agreement compared with

the experiments. The flow resistance of piles was investigated by simulating a small scale experiment as well as a full scale stabilization of a creeping slope. The results show a good agreement with the field measurements. Creep motion of a slope interacting with a shore construction foundation after the Gujarat/India earthquake was investigated, and a numerical approach was proposed. Alternating loading of a model pile was presented experimentally and numerically. It was shown that the proposed models are suitable to evaluate the interaction of piles and soft soils in static and dynamic problems.

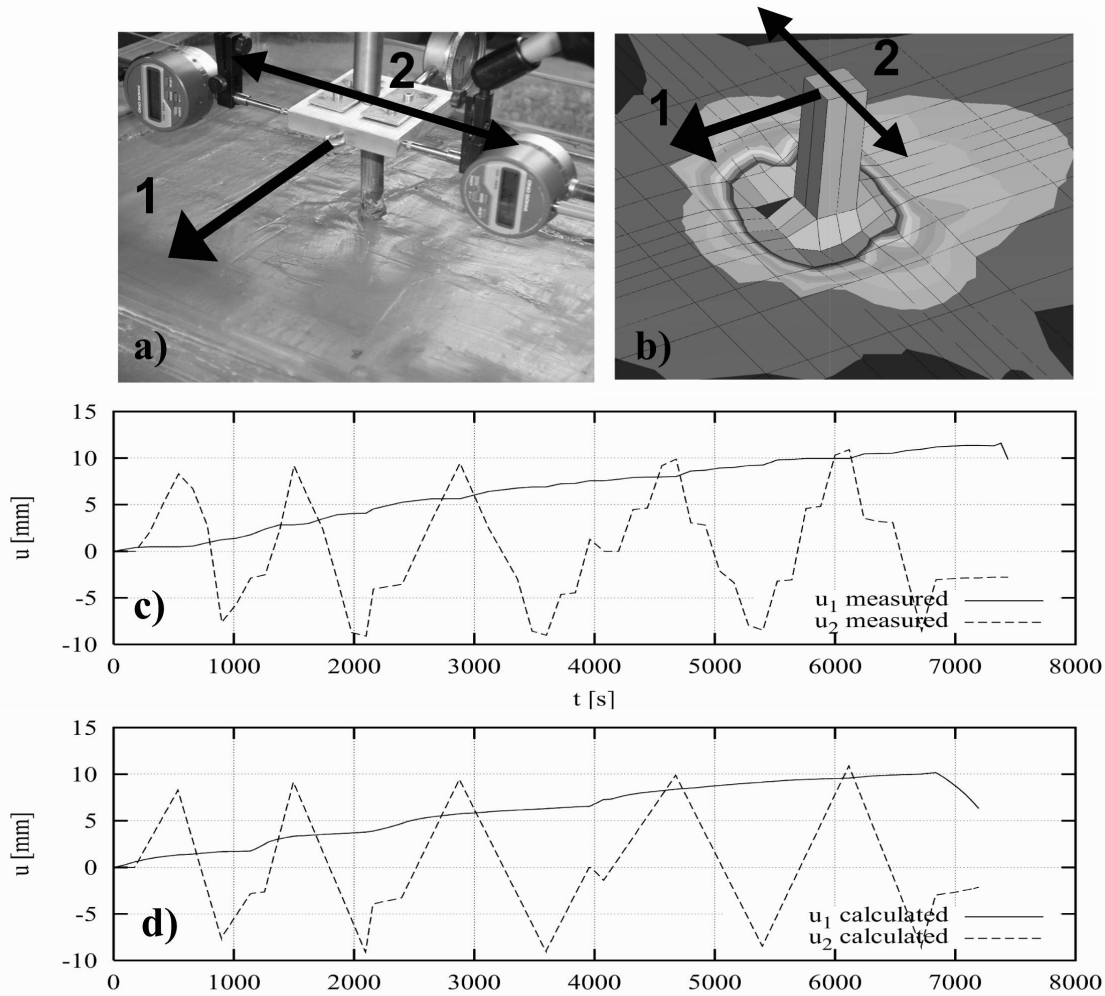


Fig. 29: Model pile in soft clay (a), finite element model (b), measured (c) and calculated (d) displacements of the pile head.

REFERENCES

- [1] BAUER, E. (1996): Calibration of a comprehensive hypoplastic model for granular materials. *Soils and Foundations* 36 (1996), No. 1, pp. 13-26.
- [2] BUISMAN, A. S. K. (1936): Results of long duration settlement tests. *Proc. 1st Int. Conf. Soil Mech. Found. Eng.*, Cambridge, 1, 103-105.
- [3] BUTTERFIELD, R. (1979): A natural compression law for soils (an advance on e - $\log p'$), *Géotechnique* 29.

- [4] CUDMANI, R., OSINOV, V. A. (2001): The cavity expansion problem for the interpretation of cone penetration and pressuremeter tests. *Can. Geotech. J.* 38, 622-638.
- [5] GUDEHUS, G. (2003): A visco-hypoplastic constitutive relation for soft soil. *Soils and Foundations*.
- [6] HERLE, I., GUDEHUS, G. (1999): Determination of the parameters of a hypoplastic constitutive model from properties of grain assemblies. *Mech. Cohesive-frictional Mater.*, 4, 461-486.
- [7] HVORSLEV, M. (1960): Physical components of the shear strength of saturated clays. Shear strength of cohesive soils, 1960, proceedings of ASCE Research Conference, Boulder, Colorado.
- [8] KOLYMBAS, D. (1978): Ein nichtlineares viskoplastisches Stoffgesetz für Böden (A non-linear viscoplastic constitutive law for soils). Ph.D. thesis, Institut für Boden- und Felsmechanik, Universität Karlsruhe, 1978.
- [9] KUNTSCHE, K. (1982): Materialverhalten von wassergesättigtem Ton bei ebenen und zylindrischen Verformungen (Material behavior of watersaturated remoulded clay under plane and cylindrical deformation). Veröffentlichungen des Instituts für Boden- und Felsmechanik der Universität Karlsruhe, dissertation, 1982, No. 91.
- [10] LEINENKUGEL, H. J. (1976): Deformations- und Festigkeitsverhalten bindiger Erdstoffe, Experimentelle Ergebnisse und ihre physikalische Deutung (deformation and shear strength behavior of cohesive soils, experimental results and their physical interpretation). Veröffentlichungen des Instituts für Boden- und Felsmechanik, Universität Karlsruhe, 1976, No. 166.
- [11] MATSUOKA, H., NAKAI, T. (1977): Stress-strain relationship of soil based on the SMP. Proc. IX International Conference Soil Mechanics and Foundation Engineering, Speciality Session 9, Tokyo, pp. 153-162, 1977.
- [12] NIEMUNIS, A., Herle, I. (1997): Hypoplastic model for cohesionless soils with elastic strain range. *Mech. Cohesive-frictional Mater.*, 2(4): 279-299.
- [13] NIEMUNIS, A. (2003): Extended hypoplastic models for soils. Heft 34, Schriftreihe des Inst. f. Grundbau u. Bodenmechanik der Ruhr-Universitaet Bochum.
- [14] NORTON, F. (1929): The creep of steel at high temperatures. McGraw Hill Book Company, Inc., New York, 1929.
- [15] SCHWARZ, W. (1987): Verdübelung toniger Böden (dowelling of clayey soils). Veröffentlichungen des Instituts für Boden- und Felsmechanik, Universität Karlsruhe, 1987, No. 105.
- [16] SOMMER, H. (1978): Zur Stabilisierung von Rutschungen mit steifen Elementen. Berechnungen und Messungen. *Die Bautechnik*, 9, 304-311.
- [17] WENZ, K.-P. (1963): Über die Größe des Seitendruckes auf Pfähle in bindigen Erdstoffen (about the extent of lateral pressure on piles embedded in cohesive soils). Veröffentlichungen des Instituts für Boden- und Felsmechanik, Universität Karlsruhe, 1963, No. 12.
- [18] WINTER, H. (1979): Fließen von Tonböden: Eine mathematische Theorie und ihre Anwendung auf den Fließwiderstand von Pfählen (Flow of clay: a mathematical theory and its application to the flow resistance of piles). Veröffentlichungen des Instituts für Boden- und Felsmechanik der Universität Karlsruhe, dissertation, 1979, No. 82.
- [19] WINTER, H. (1980): Bemessung von Pfahlgründungen und Hangverdübelungen auf Fließdruck (Design of pile foundations and piles in slopes with respect of their flow resistance). Baugrundtagung 1980, Mainz, pp. 539-563.
- [20] WOLFFERSDORFF, P. A. v. (1996): A hypoplastic relation for granular materials with a predefined limit state surface. *Mechanics of Cohesive-Frictional Materials 1: 1996*, pp. 251-271.